Chapter 2

Surface Energy-Modulated Inkjet Printing of Semiconductors

Xianghua Wang, Miao Yuan and Mengzhi Qin

Additional information is available at the end of the chapter

http://dx.doi.org/10.5772/63425

Abstract

Small-molecule organic semiconductors and quantum dots stabilized with organic surface ligand are drawing attention in future generation solution-processed devices because of their solubility in miscellaneous solvents. Solvent processing and device performance can be effectively modulated with a surface modification layer on the substrate or via ink formulation. Characterization of surface property, specifically the surface energy of the substrate and the liquid, is essentially informative. Investigation on film growth and assembling behavior as well as process optimization via surface energy modulation is successfully achieved.

Keywords: surface energy, inkjet printing, OTFT, interface nucleation, quantum dot

1. Introduction

Inkjet printing is employed as an additive direct writing material growth technology for micron scale pattern formation at a low cost and with the capability of large-scale manufacturing. It permits large-area application without the need of wetting all over the substrate, leading to minimum material consumption. Currently, it is a candidate technology to fabricate electronics of moderate performance and reliability. However, reproducibility of the process over different runs and the reliability of the fabricated devices depend on the ink formulation, the chemical and physical properties of the nozzle plate and the substrate, as well as other process conditions. The wide application of inkjet printing requires a pertinent ink solution designed for each printing step.

Due to the liquid environment, process development for inkjet printing is more complicated than that for material growth within a vacuumed chamber. Current knowledge on the material growth behavior and the mechanism in a solvent environment, especially when the material is deposited as micron scale droplets, is inadequate to satisfy the requirement of rapid process development. Research on typical inkjet-printed electronics and optoelectronics such as organic thin-film transistors (OTFTs) and pixelated color conversion coatings is originally impelled by commercial applications. Investigation of film growth via printed droplets, however, is likely to further unveil the mechanics of solvent processing in the micron and nanometer scales, which can be totally different with large-area film growth.

Concretely, organic semiconductor 6,13-bis(triisopropylsilylethynyl) pentacene (TIPS-PEN) in organic solvents and inorganic quantum dots (QDs) composed of gradient alloyed CdSe/ZnS and surface-stabilizer of PEG-COOH in aqueous solution are inkjet-printed with a Dimatix DMP3000 printer. They are potentially used as the functional layer of OTFTs and as the pixelated color conversion layer on LEDs respectively. It should be noted that the organic component or its molecular structure can be tailored for different surface energy and polarity of the semiconductor [1], thereby rendering its solubility in organic solvents or capability of patterning on a specific substrate. Similarly, the surface of the substrate for printing can be modulated by an organic monolayer with desired surface property to satisfy the requirement of inkjet printing on complex substrates, such as those with 2D patterns or 3D profiles. Fabrication of electronic devices with serial solution processing steps would also become possible [2–4].

A methodology of process development is formulated primarily based on the modulation of surface energy, which is measurable for a liquid droplet or a solid surface [5]. In the first part, also the major part, TIPS-PEN is evaluated as the channel semiconductor of OTFTs. The performance is found to be determined by the interface property as well as the crystallinity. Both can be controlled and optimized via a surface modification layer. In the second part, gradient alloyed CdSe/ZnS QDs are printed as pixelated color conversion element. Here results on an aqueous solution of green color QDs is discussed and referred to as green QDs. In this application, the higher surface energy of aqueous QD solution is favourable to stable jetting. Therefore, positioning accuracy and repeatable printing cycles are developed for accumulated assembling of QDs, while the footprint is well confined within the coffee-rings of the anteriorly printed PVP underlying layers.

2. Small-molecule organic thin-film transistor

Solution processing of soluble conjugated molecules at low cost is a key technology to fabricate OTFTs for “printed electronics”. Small-molecule organic semiconductors exhibit high field-effect mobility as a single crystal. The intrinsic field-effect mobility approaches 1 $cm^2V^{-1}s^{-1}$ or even higher than 10 $cm^2V^{-1}s^{-1}$, which is comparable or even superior to those of hydrogenated amorphous silicon (a-Si:H). Compared to polymer semiconductors, small molecule can form low viscosity solutions, which is conducive to stable jetting. Furthermore, the switching

performance of small-molecule OTFTs is usually superior to that of the polymer devices, typically showing a small subthreshold swing (SS). Therefore, much attention is devoted to material processing of small-molecule organic materials in solution forms.

As to the application in OTFTs, we are especially interested in the surface coverage on the substrate, the crystalline morphology, and interface quality. A well-studied small-molecule semiconductor, TIPS-PEN, is used as the semiconducting layer of OTFTs and deposited by inkjet printing. The jetting waveform as shown in **Figure 1** is optimized for stable jetting at frequencies lower than 2 kHz.

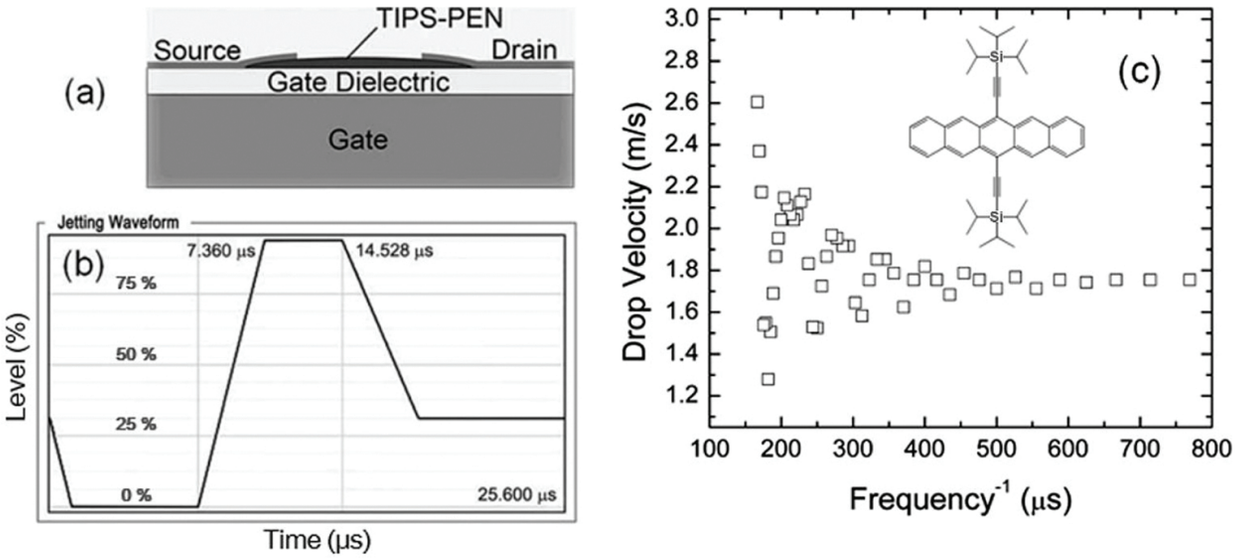

Figure 1. (a) Schematic diagram of a bottom-gate/top-contact OTFT with inkjet printed TIPS-PEN as the channel semiconductor, (b) The 3-segment jetting waveform, (c) Drop velocity at different jetting frequencies; the inset shows the molecule structure of TIPS-PEN.

2.1. Morphology of single-drop films

A silicon wafer with 300 nm thermal oxide is used as the substrate for inkjet printing. A simple solvent cleaning process is performed on the substrate, which consists of 3 min of ultrasonic cleaning in acetone followed by an ethanol rinse and blow-dry with N_2. In addition to solvent cleaning, spin-coated hexamethyldisilazane (HMDS) is employed to modify the surface property of the substrate. Another surface treatment method uses 10 min of UV-ozone treatment instead of the HMDS coating. Surface tension of liquids and their contact angle with the surface-treated substrate are measured with a type OCA15 video-based automatic contact angle measuring instrument from Data Physics. The surface energy of the substrates as shown in **Figure 2** is calculated from the contact angle measured at a room temperature of 25°C. The surface energy including the dispersion component γ_s^d and the polar component γ_s^p are evaluated based on contact angle measurements of de-ionized water and methylene iodide on these substrates using the harmonic-mean model of Wu [6].

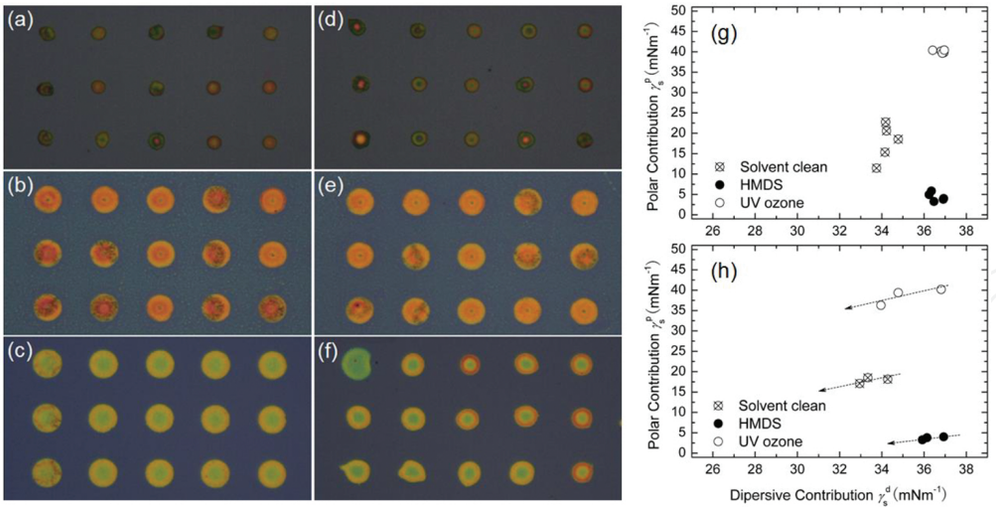

Figure 2. Optical microscopy of arrayed single-drop films on surface treated silica substrate using a 2 wt% TIPS-PEN solution dissolved in *o*-DCB. Drop spacing is 150 μm. (a, d) printed on solvent-cleaned wafer, (b, e) on HMDS-treated wafer, (c, f) on UV-ozone cleaned wafer, after air exposure of 2 hours and 4 hours respectively. (g) Dispersive and polar component of surface energy measured from solvent cleaned wafer and surface-treated substrates. (h) Evolution of surface energy with different air exposure time from 2 to 6 hours.

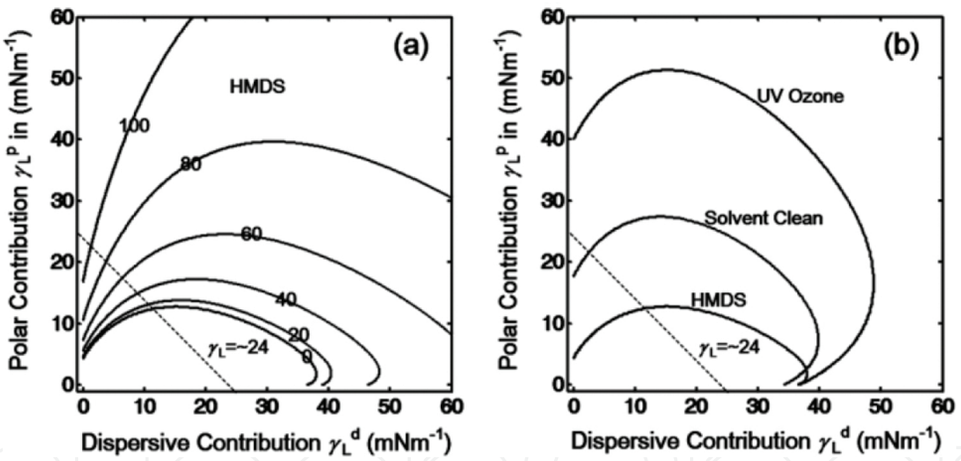

Figure 3. (a) Wetting envelope contour of HMDS-treated substrate plotted for different contact angles (0°–120°); (b) 0° contours for substrates after different surface treatment.

At an ambient temperature of 25°C, the measured surface tension of a 2 wt% and a 1 wt% TIPS-PEN ink solution is 24 mNm^{-1} and 24.4 mNm^{-1} respectively, while that of pure *o*-DCB solvent is 24.8 mNm^{-1}. Contact angle of 2 wt% TIPS-PEN solution on the UV-ozone cleaned sample was 0° at room temperature, while that on an HMDS-treated substrate is about 12°. From the wetting envelope contours shown in **Figure 3**, it is estimated that the solution have a dispersive surface energy of 11.5 mNm^{-1} and the polar component is 12.5 mNm^{-1}, very close to the intersection of the dash line and the 0° contour of the HMDS-treated substrate. Accordingly, the solution completely wets on both of the other two substrates. Obviously, the difference in single-drop film diameter is not determined by the degree of wetting. Further experiment

results in the following sections indicate a positive correlation between single-drop film diameter and the dispersion portion of the substrate's surface energy, which agrees with the results in **Figure 2** and well explains the air exposure effect.

2.2. Elimination of coffee ring staining via surface processing

Apart from film diameter, the thickness profile is evaluated. To achieve a high surface coverage and crystalline film of uniform thickness, the coffee ring phenomena, which is ascribed to faster solvent evaporation from the periphery of the liquid surface, should be avoided. The coffee ring profile can be restrained by slowing down the outward flow induced by solvent evaporation, or by inducing a reverse flow with a gradient of surface tension, which can be achieved by a co-solvent system. Another effective approach relies on a facile surface energy modulation of the substrate [7]. The effectiveness arises from the relatively strong interaction between the substrate and the solute molecules, so that the film deposition is initiated by heterogeneous nucleation on the liquid-substrate interface instead of the localized concentration saturation as a result of the higher solvent evaporation rate on the periphery.

Surface silanization with a SAM layer of perfluorodecyltrichlorosilane (FDTS) effectively reduces the surface energy of SiO_2. While the FDTS-SAM treatment reduces the dispersion component as well as the polar component of the surface energy, surface cleaning such as UV-ozone cleaning is found to selectively enhance the polar contribution of surface energy. The combination of a FDTS-SAM treatment and UV-ozone cleaning is proven to be effective in tuning the diameter and profile of the printed single-drop films. For comparison, two sets of surface treatments are performed and the corresponding surface energy is measured. One is solely treated with UV-ozone cleaning and the other is pre-treated with a FDTS-SAM treatment. **Figure 4(a)** and **(b)** respectively shows their surface energy in a two-dimensional coordinate space (polar component and dispersive component). Dependence of surface energies, including their two components, on the treatment time of UV-ozone cleaning is plotted in **Figure 4(c)** and **(d)**, respectively, for the two sets of surface treatments.

As shown in **Figure 4(d)**, a prior FDTS-SAM treatment significantly improves the responsivity of surface energy on the treatment time of UV-ozone cleaning. Therefore, the combination of FDTS-SAM treatment and UV-ozone cleaning provide more effective modulation of the surface energy and the film morphology printed thereon. For substrates treated with UV-ozone cleaning alone, the dispersive component and the polar component are of comparable magnitude. For the FDTS-treated sample, the two components deviate from each other after 6 min of UV-ozone cleaning. The strongest contrast is noticed after 8 min of UV-ozone cleaning, when the polarity is maximized to 0.71 for the FDTS-treated sample. Nevertheless, for both sets of substrates, the total surface energy saturates at almost identical level of 75 mNm^{-1}. Based on the differential surface energies, a comparative study on inkjet printing is performed on two SiO_2/Si samples, one of which is solely surface-treated with 8 min of UV-ozone cleaning (S1) while the other is grown with a FDTS-SAM followed by the same treatment of 8-min UV-ozone cleaning (S2). It should be noted that these surface treatment cannot achieve a hydrophobic surface.

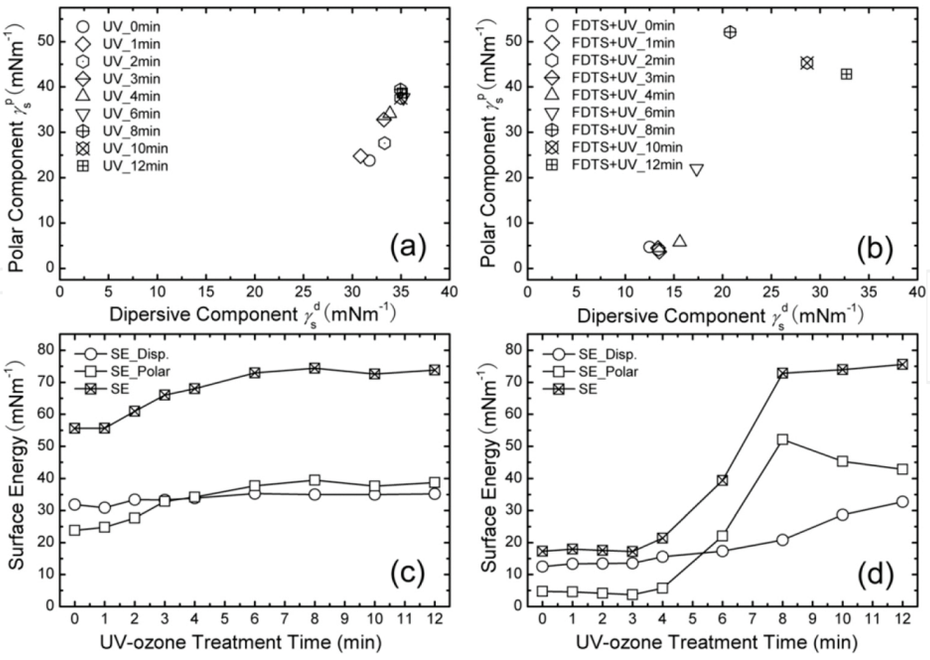

Figure 4. Surface energy of SiO_2 plotted in coordinates of polar component versus dispersive component (a, b), and their dependence on the treatment time of UV-ozone cleaning (c, d).

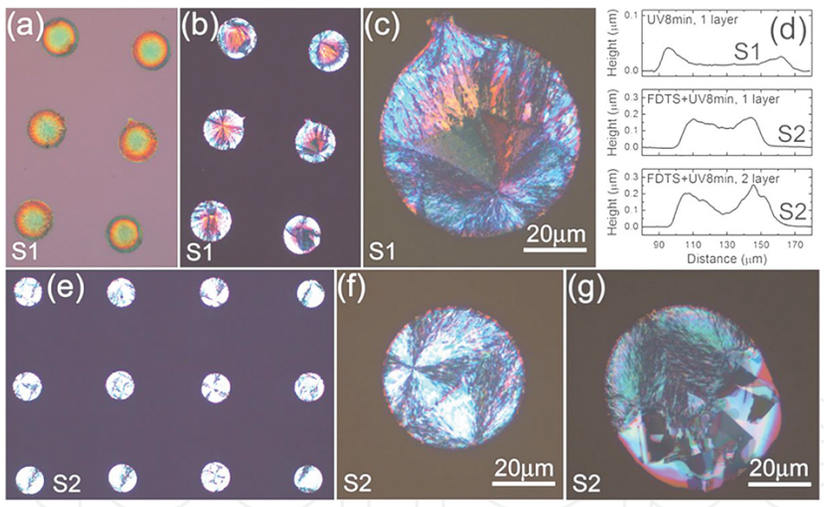

Figure 5. Single-drop films on SiO_2 with different surface processing. (a-c) UV-ozone-treated SiO_2, (d) PVP-coated substrate, (e, f) FDTS-SAM followed by UV-ozone treatment; (g) microphotograph of a 2-layer isolating dot printed with 2 shots on the same site at a time interval of 10 s.

The polar contribution of surface energy is found to be responsible for the coffee ring profiles, which is usually more serious at increased substrate temperatures or increased number of droplet impacts at the same site (**Figure 5(d)**). On hydrophobic surfaces, such as a PVP-coated or a PETS-treated substrate, more uniform film thickness is obtained as shown in **Figure 6**. We also note that the coffee ring profile would not appear on these hydrophobic substrates even at elevated substrate temperatures.

http://dx.doi.org/10.5772/63425

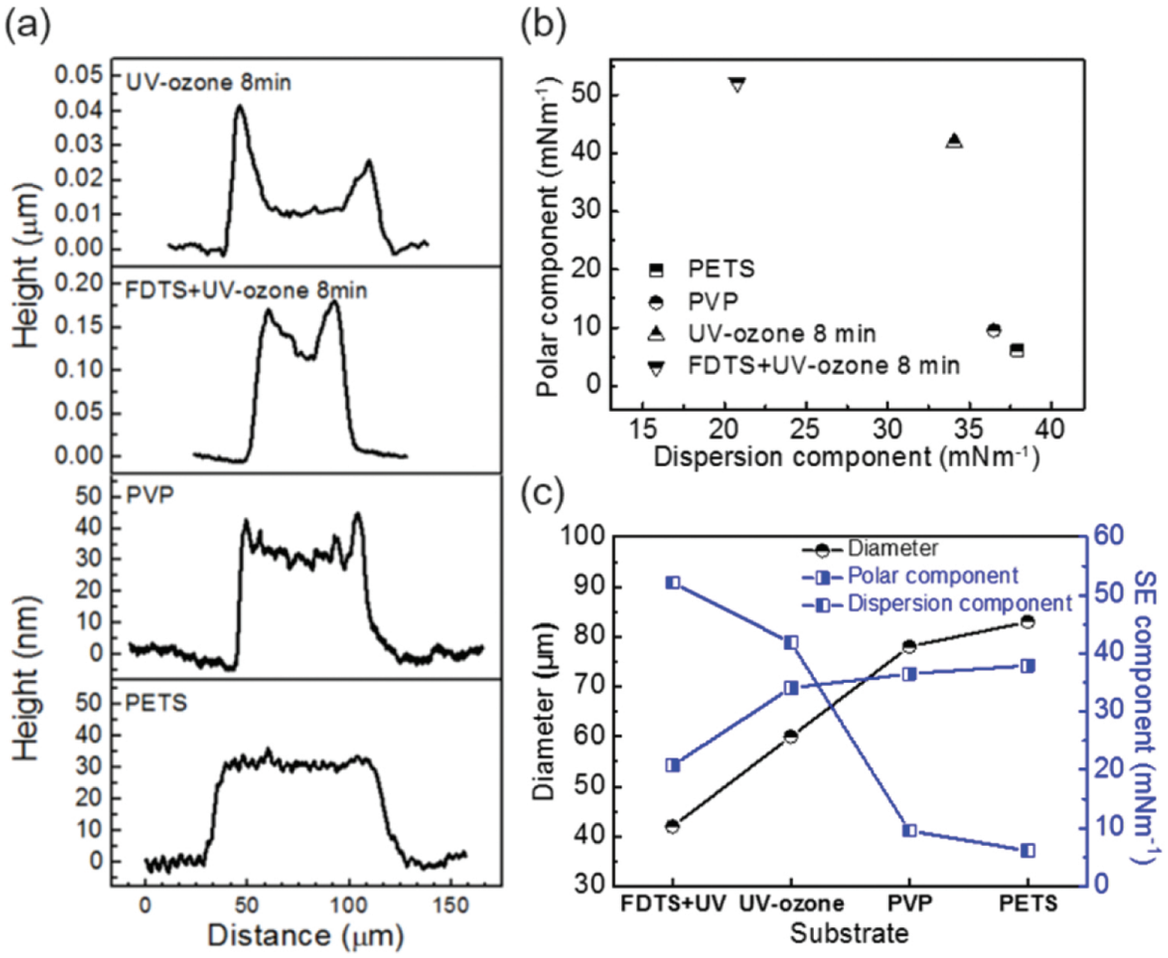

Figure 6. Modulation on thickness profile of a single-drop film via surface processing. The film is printed via *o*-DCB.

2.3. Process optimization for top-contact OTFTs

Fabrication of the field-effect transistor starts with an n-type Si wafer as the common gate material, and a 300 nm thermal oxide is employed as the gate insulator (capacitance =10.8 $nFcm^{-2}$), whose surface property is considered to be a critical factor that controls the morphology of the printed semiconductor. Instead of pursuing a high resolution patterning, printing of the semiconductor is performed at relatively low resolution, while finer electrode pattern is defined with standard photolithography. Of course, the fabrication of metal line and source-drain electrodes can as well be directly patterned with inkjet printing [8]. In this chapter, the source-drain electrodes are grown by thermal evaporation and patterned via a lift-off process. According to the growth sequence of the semiconductor versus the source-drain contacts, the device architecture is referred to as bottom-gate-top-contact and bottom-gate-bottom-contact respectively. Large-area TIPS-PEN films in the form of single-line or overlapping multiple-line film are employed for OTFT devices.

Single-line films were printed with a drop spacing (DS) of 20 μm. **Figure 7(a)** shows the microphotographs of the single-line film printed on S1 (left) and S2 (right) respectively. Films

of broader width have been printed as well. The inset diagram shows the digital pattern, defined by DS and line spacing (LS) for the printing of broad-width films. The upper diagram of **Figure 7(b)** shows the cross-section profile of the single-line films (intersected by a plane normal to the *y*-direction), showing a concave profile in the middle due to coffee-ring effect. The lower diagram shows the cross-section profile across a wider line printed with two runs along the *y*-direction shifted by an LS of 160 μm in the *x*-direction, which is obviously unsymmetrical, being thicker on one side than the other.

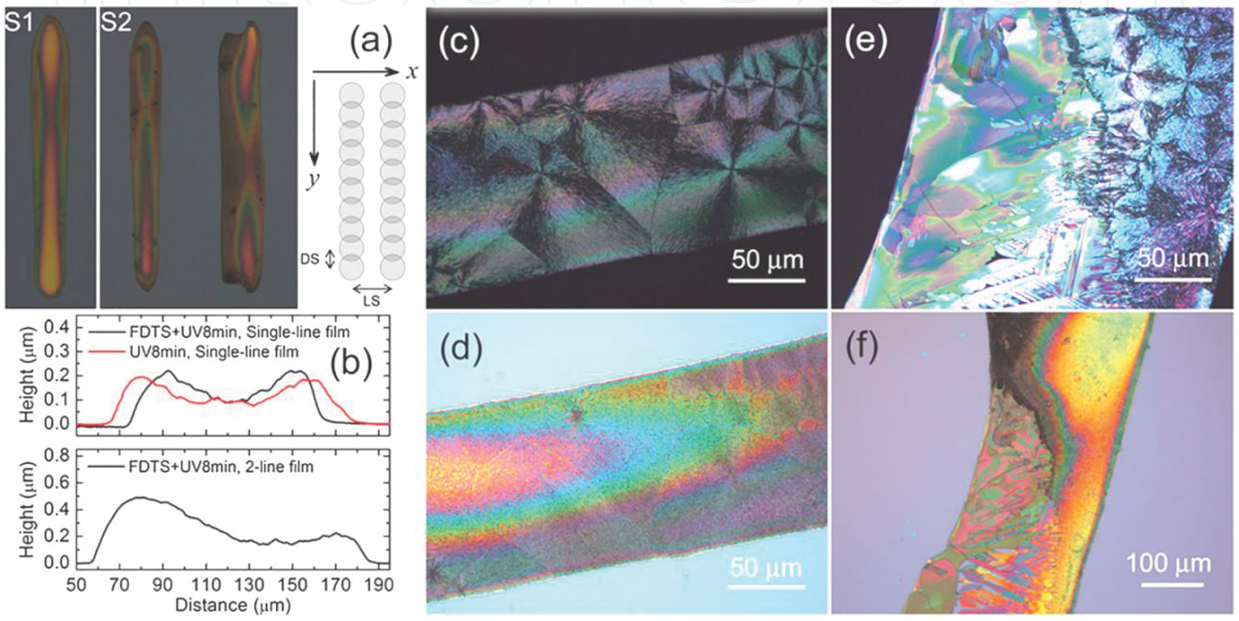

Figure 7. Microphotographs and cross-section profiles of single-line, overlapping 2-line, and multiple-line films of TIPS-PEN printed on SiO_2. (a) Image taken with the fiducial camera of the printer (left: single-line film on S1; right: single-line and 2-line films on S2.) The inset diagram shows the printing parameters, DS and LS, as defined for the pattern. (b) Profiles of the single-line films and the 2-line film as shown in (a). Cross-polarized (c, e) and unpolarized (d, f) microphotographs of the films printed on the SiO_2 that is surface modified with a FDTS-SAM treatment followed by 8 min (c, d) and 10 min (e, f) of UV-ozone cleaning respectively. Films in (c, d) and (e, f) are printed with 2 and 4 overlapping lines respectively.

The substrate for OTFT fabrication is fluorinated with FDTS followed by 8 min of UV-ozone cleaning. A single nozzle is used for the printing of single-line films or large-area films with overlapping-drop assignment. The print head performs a forward single-trip movement along the *y*-direction printing a single line with a specified DS that is smaller than the single-drop diameter. At the ending of the forward trip, the print head stops jetting and returns to its starting position on standby or move a step distance along the *x*-direction according to the specified LS. Films of broader widths were printed by repeating the round trip shifted by an LS smaller than the single-line width. OTFT arrays are printed using varied DS and LS, and optimization on these parameters can contribute to better device performance. As shown in **Figure 8**, the result suggests a critical dependence of field-effect mobility with film thickness and an optimal LS/DS ratio can enhance current on/off ratio of the OTFT by a factor of 10.

http://dx.doi.org/10.5772/63425

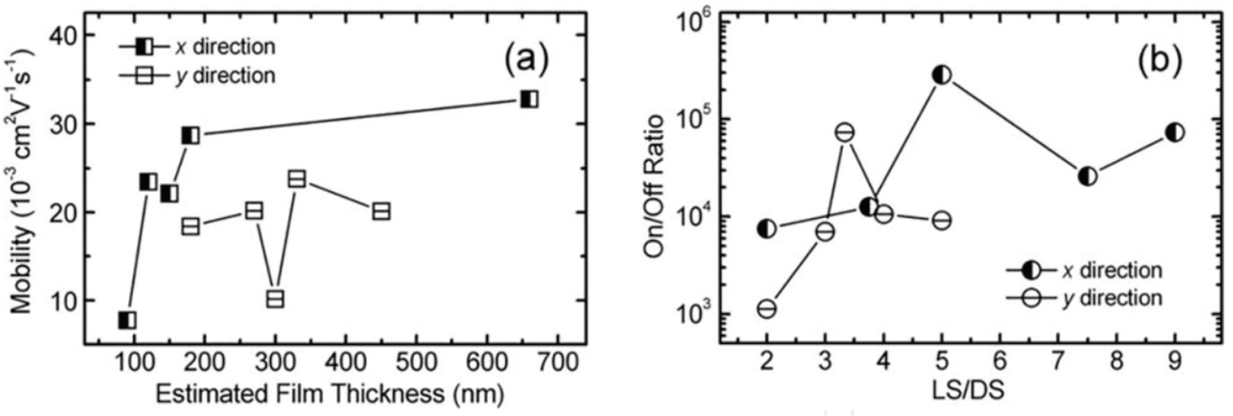

Figure 8. Saturated field-effect mobility of inkjet-printed TIPS-PEN via an *o*-DCB solution on SiO_2 substrates treated with FDTS-SAM and 10 min UV-ozone Cleaning. (a) Dependence of mobility along *x*- and *y*-direction on film thickness; (b) Dependence of on/off ratio for field-effect charge transport along *x*- and *y*-direction on the ratio of LS/DS.

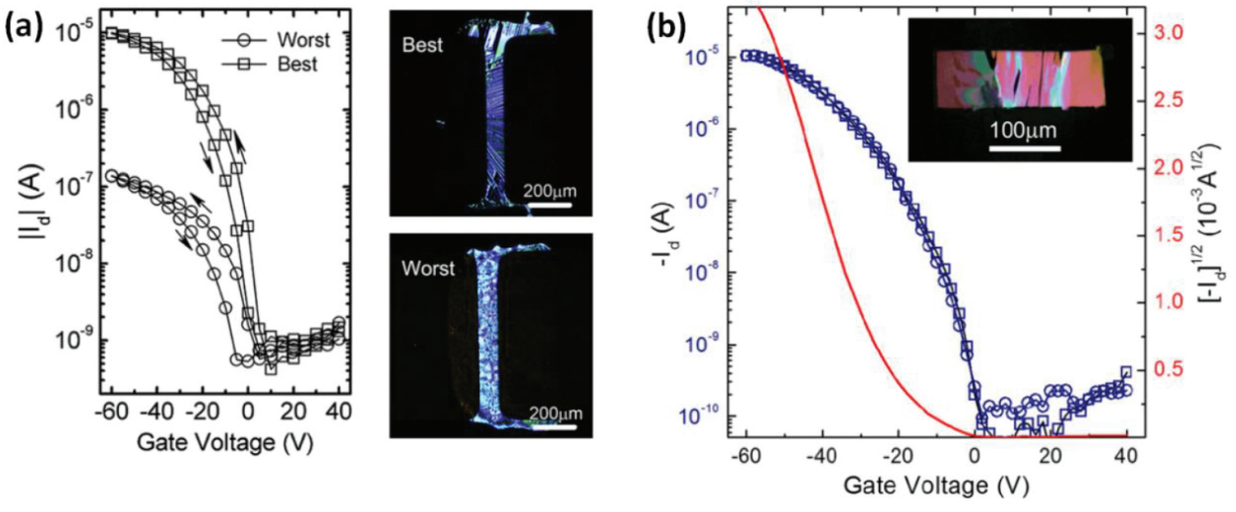

Figure 9. (a) Transfer curves under cycle-swept V_g and the cross-polarized microscopy of the best and the worst device within the same line of the printed OTFT arrays on PVP/SiO_2 substrate, both devices are printed via *o*-DCB; (b) Transfer curves under cycle-swept V_g of the highest performance device printed via tetralin, with the accumulation curve shown in open squares and depletion curve in open circles, Inset: the cross-polarized microphotograph of the OTFT.

The effect of using a hydrophobic dielectric surface is also investigated. By spin-coating a second dielectric layer of PVP on the SiO_2 as the dual layer gate dielectric, the field-effect mobility can reach 0.1 $cm^2V^{-1}s^{-1}$, but the average mobility is not as high due to the lower performance of devices in the first few columns. Apparently, the difference has been caused by the contrastive film morphology as shown in **Figure 9(a)**. Dissolution test indicates a poor compatibility of the cartridge material with *o*-DCB, which would lead to inferior device performance after a process idle. This is a serious problem in developing high performance devices. Milder solvent such as toluene, anisole, xylene, and tetralin are potential candidates as the solvent. Of these, tetralin is more promising for inkjet printing via tiny droplets because

of its high boiling point that favours self-organization of the semiconductor molecules as crystalline films.

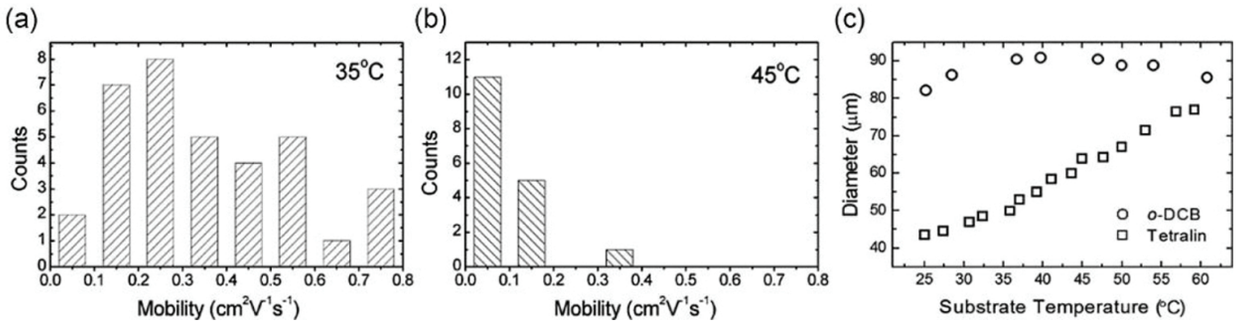

Figure 10. Mobility distribution of 54 TIPS-PEN OTFTs fabricated on PVP/SiO_2 substrate with the semiconductor inkjet printed via a 2 wt. % solution in tetralin. Inkjet printing was conducted with the substrate temperature maintained at 45°C (18 devices) or 35°C (36 devices); Diameters of single-drop films printed via the single-solvent solution of *o*-DCB or tetralin on PVP-coated substrate with increasing substrate temperature.

The multi-line film of TIPS-PEN printed via tetralin on a PVP/SiO_2 substrate is polycrystalline with domains in the shape of wide strips (20–100 μm in width) when printed at a substrate temperature of 35°C. The crystal growth direction runs parallel with the *y*-direction of the printed pattern, therefore, top-contact/bottom-gate OTFT architecture is fabricated with the channel perpendicular to the *y*-direction of the printed film. Devices printed at a lower substrate temperature of 35°C are generally superior to those printed at a higher temperature of 45°C. The average mobility of devices printed at 35°C is enhanced by one order of magnitude to a value of 0.36 $cm^2V^{-1}s^{-1}$ compared with those printed with the *o*-DCB ink, while the maximum mobility reaches 0.78 $cm^2V^{-1}s^{-1}$, which is about a 7-fold increase. The threshold voltage is -21 V as estimated from the transfer curve in **Figure 9(b)**. Mobility distribution of these OTFTs is shown in **Figure 10**. OTFTs printed at 35°C outperform those printed at 45°C owing to the larger film thickness. Also shown in **Figure 10(c)**, the increasing diameter of the single-drop film printed via tetralin indicates a decreasing film thickness with increasing substrate temperature. Among the 36 devices printed at 35°C, 35 devices exhibit typical OTFT characteristics with approximately 95% of the devices falls within the range of 0.1–0.8 $cm^2V^{-1}s^{-1}$. Compared to devices printed with an *o*-DCB ink, the tremendous improvement in mobility as well as the more uniform device performance is at least partially ascribed to the tetralin solvent that possesses a higher surface energy than *o*-DCB, providing a wider process window for the tuning of single-drop film diameter and film thickness.

Film coverage of TIPS-PEN films inkjet-printed for top-contact OTFTs is characterized with AFMs as shown in **Figure 11**. Almost 100% material coverage within the domains was observed for samples printed with the 2 wt% tetralin solution on the PVP/SiO_2 substrate. When a 2 wt % solution using *o*-DCB as the solvent, the crystal ribbons become narrower in width and are

not fully grown, but the crystal growth direction is well aligned. In contrast, crystal domains are not as well aligned over large areas on an untreated hydrophilic SiO_2 substrate.

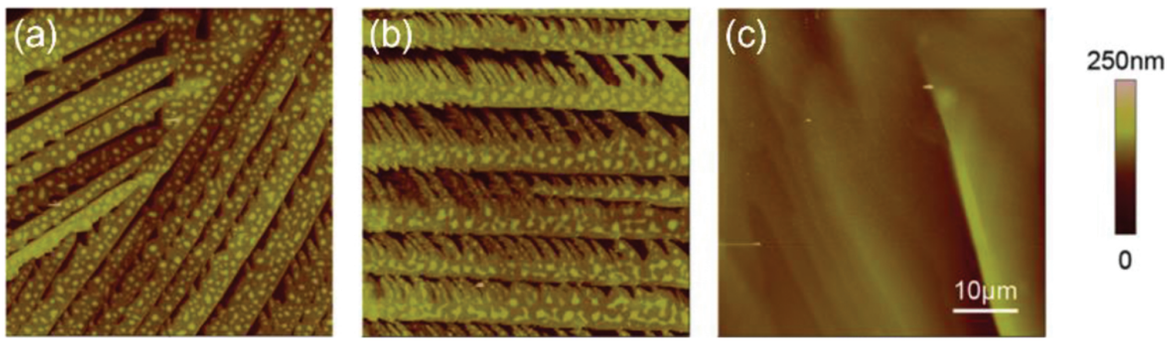

Figure 11. AFM images (50×50 μm²) of large-area TIPS-PEN films printed with overlapping multiple lines on 3 substrates (Left: via *o*-DCB on untreated hydrophilic SiO_2, Middle: via *o*-DCB on PVP/SiO_2, Right: via tetralin on PVP/SiO_2).

2.4. Dielectric surface treatment for bottom-contact OTFTs

The crystallinity of small-molecule semiconductor is generally known to be of paramount importance to its electrical property. Hasegawa et al. developed an antisolvent crystallization inkjet printing technique for the fabrication of single-crystal films on a substrate with predefined patterns. The method is very effective for 2,7-dioctyl[1]benzothieno[3,2-b][1]benzothiophene (C_8-BTBT), achieving average field effect mobility as high as 16.4 $cm^2V^{-1}s^{-1}$. However, the effectiveness is found to be critical on the type of the semiconductor material as to their preferred crystallization behavior. Direct printing of high performance TIPS-PEN OTFTs is still a challenge. The primary obstacle firstly lies in the relatively low field-effect mobility of bottom-contact devices, which is still much smaller than 1 $cm^2V^{-1}s^{-1}$; and secondly, the relatively large subthreshold slope, typically larger than 2 V per decade. The gap can be explained by the inferior crystalline morphology and interface quality. Organic single-crystal transistors can be directly printed on a surface-energy patterned substrate using a co-solvent ink that refrains coffee-ring deposition [9]. To facilitate single-domain crystal growth from a solution, technique of wetting/nonwetting patterning is employed to induce directional lateral crystal growth via the artificial boundary.

In most circumstances, pinning of the three-phase contact line (TCL) initiates the nucleation and crystal growth starts from the circumference and result in polycrystalline film morphology usually with coffee-ring profile. Physical models are proposed to explain the evaporation-induced self organization [10]. However, for the printing of organic semiconductors, it is still difficult to set up an accurate model for the evaporation process based on the contact angle hysteresis measured by a classical method. Because the contact angle, pinning diameter and receding distance are found to be dependent on various factors such as droplet size, solute concentration, and the contact line velocity [11]. It is observed that the receding contact angle determines the TCL behaviors, and can be successfully employed for the assembling of photonic crystals into a dome structure [12]. However, the target of organic semiconductor

film growth is clearly different: laminated structure is desired instead of coffee ring profile or dome structure. It relies to a great extent on the nucleation and its preferred crystal growth behavior to self-organize the solute molecules into the laminated structure.

Printing of bottom-contact OTFTs have to take into account the surface effect of contact electrode in addition to the dielectric surface. In the following, we focus on the latter factor, which is investigated by modifying the surface with a SAM layer of phenethyltrichlorosilane (PETS) or phenyltrichlorosilane (PTS), a spin-coated PVP layer or a UV-ozone treatment. Pentafluorothiophenol (PFTP) was used for the surface treatment of Au electrode. The surfaces as prepared are characterized by contact angle measurement as shown in **Table 1**.

	PTS	PETS	PVP	UV-Ozone	Au	PFTP-Au
CA of H_2O (°)	87.5	85.5	71.3	31.0	91.8	85.4
CA of CH_2I_2 (°)	35.5	37.5	34.4	36.5	23.7	28.6
γ_d (mN·m-1)	38.96	37.94	36.50	37.38	44.20	41.60
γ_p (mN·m-1)	5.17	6.13	9.56	32.47	2.80	5.60
γ (mN·m-1)	44.14	44.07	46.04	69.85	47.00	47.20

Table 1. Contact angles and surface energies of surface-modified dielectrics and Au.

Surface morphologies of the substrates are observed with AFM as shown in **Figure 12**. The surface of the spin-coated PVP and the UV-ozone-treated SiO_2 are comparable in roughness. AFM images indicate that agglomeration of the silane molecules has significantly deteriorated the smoothness of the dielectric surface. The maximum height difference is increased by approximately five times after PETS treatment with an average distance of about 50 nm between neighbouring particulates. Agglomeration of PTS molecules forms even larger particles of around 250 nm in size and dispersed with an average distance larger than 500 nm.

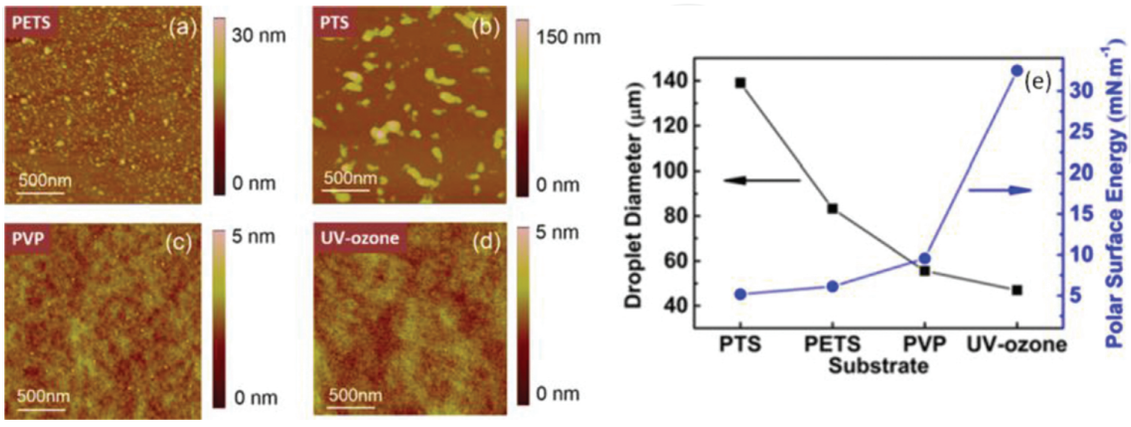

Figure 12. Surface morphology of SiO_2/Si substrates treated by a SAM layer of (a) PETS, (b) PTS, (c) spin-coated PVP, and (d) UV-ozone cleaning; (e) Polar surface energies (solid circles) of SiO2/Si substrates after different surface treatment and the average diameters (solid squares) of the single-drop films printed on them.

TIPS-PEN is printed as a single-line film with a 2 wt% solution in tetralin with the substrate temperature kept at 35°C. Surface morphologies of the single-line films printed at DS of 20 μm and 10 μm are shown in **Figure 13**. Large crystallites are obtained on smooth surfaces, while rougher surfaces as those with PETS- and PTS-treatment clearly result in grainy TIPS-PEN films, which are especially evident for thinner films printed at 20 μm DS. According to the high density of nanocrystalline formed on the SAM-treated surfaces, it is inferred that the film growth on the SAM-treated substrates has been induced by interface nucleation; however, the crystal growth mode seems to be different. Crystal growth on the PETS-treated surface follows a 2D growth mode, while the PTS-treated surface induces a 3D growth mode, which is confirmed by the contrastive height profiles especially that of the thicker films printed at a DS of 10 μm. The increase in grain size for thicker films is most remarkable on the SAM-treated substrates. The out-of-plane X-ray diffraction (XRD) patterns corroborate the dramatic increase in crystallinity for films printed with reduced DS, which is more apparent for the SAM-treated substrates.

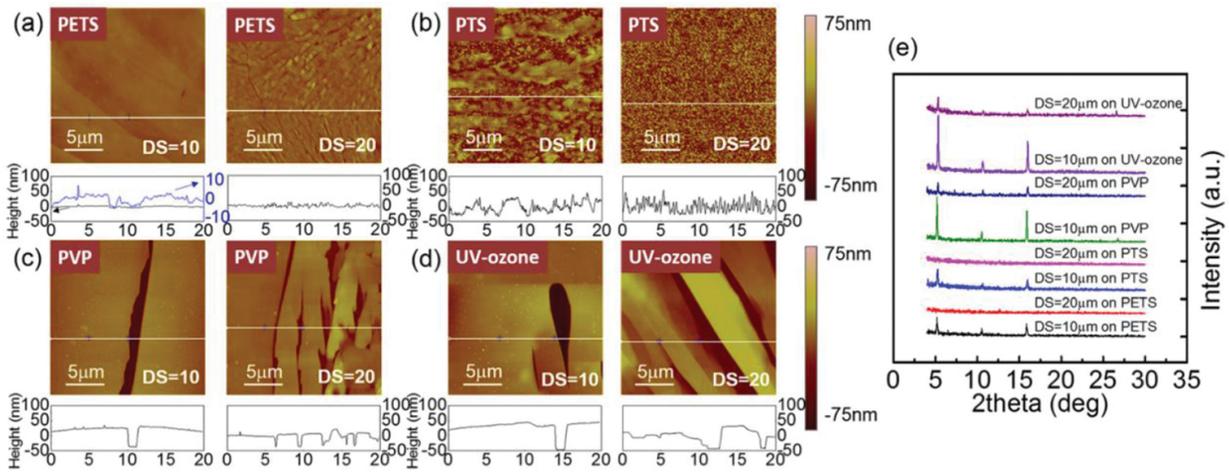

Figure 13. Surface morphologies of single-line films printed at drop spacing of 10 μm and 20 μm on SiO_2/Si substrates with different methods of surface treatment (a) PETS, (b) PTS, (c) PVP coating, and (d) UV-ozone cleaning, and (e) out-of-plane XRD patterns of the films with different (00l) peak intensity.

Bottom-contact OTFTs is prepared by printing the TIPS-PEN solution as a single-line film across the source-drain electrodes. As shown in **Figure 14**, the Au electrode induces crystal growth from channel boundary to the centre of the channel, which will inevitably cause a decrease of field-effect mobility. It is clearly seen from the transfer curves in **Figure 15** that the SS is incremental with increasing surface polarity. It is also notable that the OTFT prepared on PETS-treated substrate shows the best performance, with a threshold voltage as small as 1.1 V and a narrow SS of 0.85 V/decade. The extracted transistor parameters for the best performing devices are provided in **Table 2**.

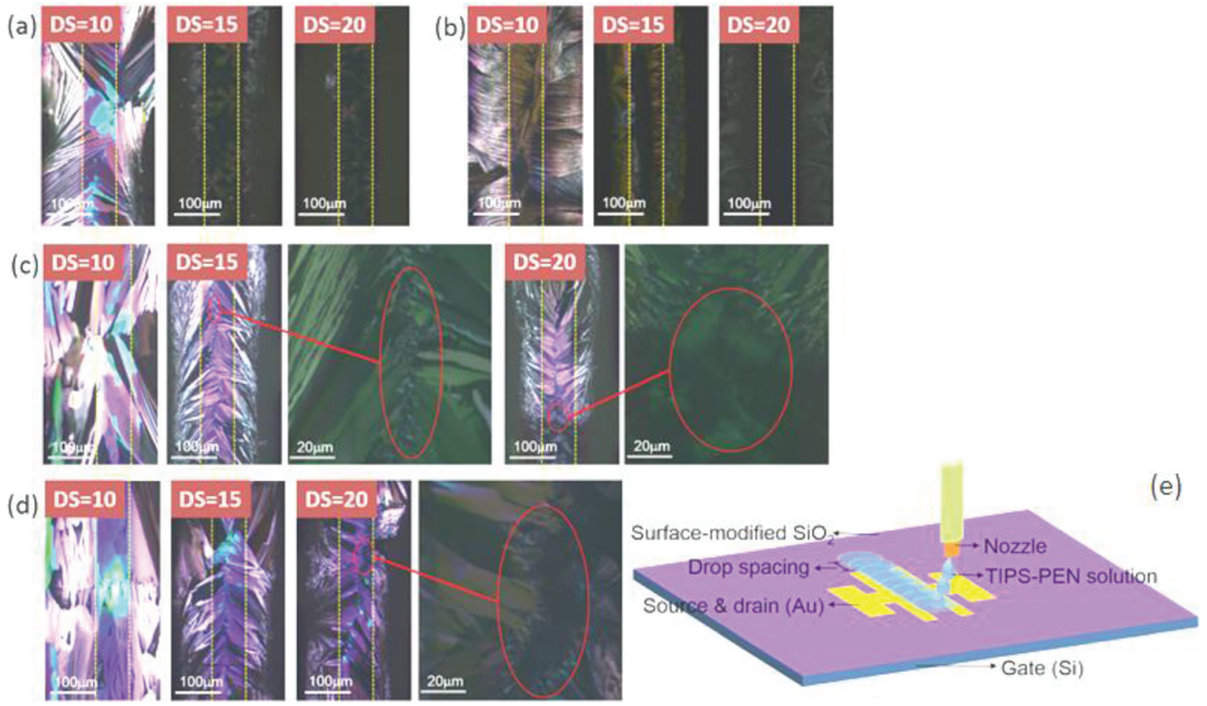

Figure 14. Cross-polarized microphotographs of bottom-contact OTFTs with the single-line films of TIPS-PEN printed across the channels. The substrates have been treated with (a) PETS, (b) PTS, (c) PVP coating, and (d) UV-ozone cleaning.(e) Schematic diagram (not to scale) of bottom-gate/bottom-contact OTFT with inkjet-printed TIPS-PEN as the semiconducting layer in the channel.

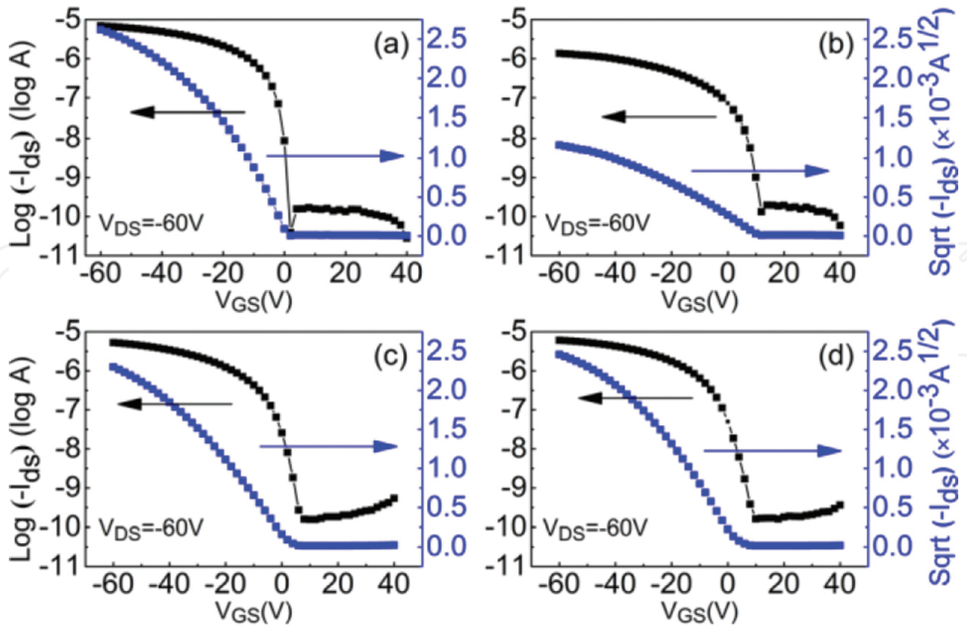

Figure 15. Transfer curves of the best-performing OTFTs. The substrates have been treated with (a) PETS, (b) PTS, (c) PVP coating, and (d) UV-ozone cleaning.

Substrate	DS (μm)	μ ($cm^2V^{-1}s^{-1}$)	V_{TH}(V)	$I_{on/off}$	SS($Vdec^{-1}$)
PETS	10	0.140	1.1	$2.5x10^5$	0.85
	15	0.030	1.0	$1.0x10^4$	1.88
	20	0.012	2.2	$3.5x10^3$	1.82
PTS	10	0.007	3.0	$2.2x10^3$	2.27
	15	0.006	2.8	$3.0x10^3$	1.68
	20	0.005	1.6	$2.4x10^3$	2.62
PVP	10	0.062	3.4	$4.1x10^4$	2.40
	15	0.047	3.5	$3.4x10^4$	3.36
	20	0.047	2.7	$2.4x10^4$	2.98
UV-ozone	10	0.058	4.3	$3.0x10^4$	3.10
	15	0.064	6.7	$2.6x10^4$	2.10
	20	0.056	5.5	$2.8x10^4$	1.34

Table 2. Device parameters of the best performing OTFTs.

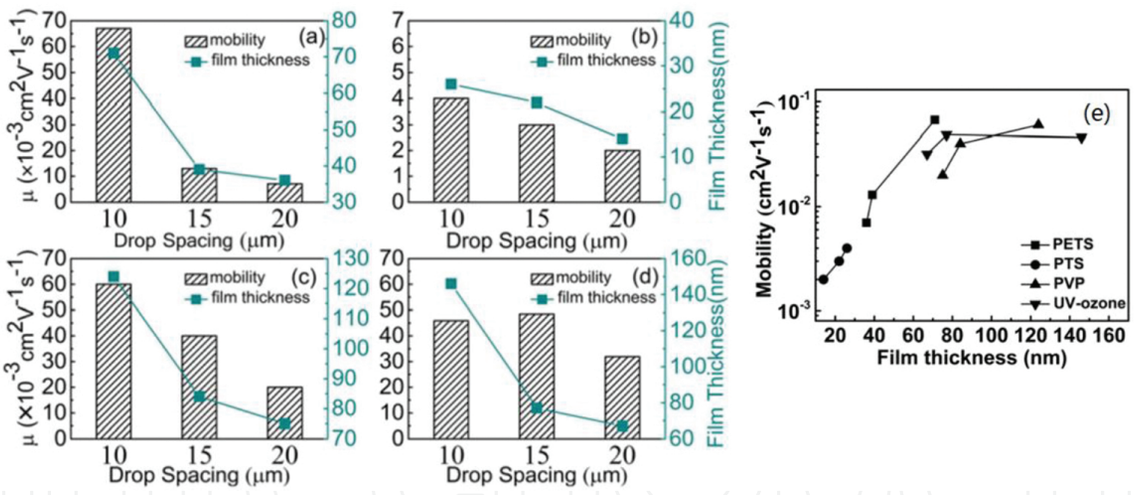

Figure 16. Dependence of film thickness and mobility on drop spacing and correlation between film thickness and field-effect mobility. The substrates have been treated with (a) PETS, (b) PTS, (c) PVP coating, (d) UV-ozone cleaning; (e) Semilogarithmic plot of mobility versus film thickness.

Figure 16 plots the dependence of field-effect mobility and film thickness on the printing parameter of DS. The field-effect mobility generally decreases as the DS is increased, which is ascribed to the decreasing film thickness and crystallinity. An exponentially-decaying trend of saturated mobility on decreasing film thickness is observed for both SAM-treated substrates in the thickness range of approximately sub 100 nm. Although thicker films can be formed on surfaces of higher polarity, the mobility is not improved following the same trend. The device performance is limited by the film morphology of TIPS-PEN showing two features as shown

in **Figure 14(c, d)**. First, the film coverage is not significantly improved with increasing film thickness; second, a crystal boundary in the middle of the channel is formed in the solidified film. Both features are caused by the contact-line nucleation behavior. This problem is not apparent for films printed on the SAM-treated substrates as interface nucleation has played a more significant role during film growth. Film growth via interface nucleation contributes to the formation of a film with higher thickness uniformity and improved crystal coverage, and therefore exhibits higher field-effect mobility.

3. Stacked layers of quantum dots for color conversion

In this part, inkjet printing is developed for the printing of the color conversion element for full-color LED displays. Fluorescent CdSe/ZnS QD is printed via several ink systems. The jetting stability is the key issue to be solved for this application. The stability of the jetting behavior is recorded by printing a dot array, from which the accuracy of drop assignment is evaluated by the extracted coordinates (**Figure 17**). Surface energy of the solvent is a critical factor for stable jetting of the ink suspension. Improvement in jetting stability of the green QDs is achieved using a mixture solvent of water and diluted acetic acid. These experiments again indicate the effectiveness of process development by modulating surface energies of the relevant materials and interfaces, including the substrate, the solvent, and the solute or the dispersed material.

The CdSe/ZnS QDs can be synthesized in organic solvents, however our experiment shows that printing of these organic ink suspension is unstable. The low surface energy of the typical organic solvent for QDs, such as hexane or toluene, substantially wets on the hydrophobic nozzle plate. The single-solvent system of these QDs may not jet at all. The suspension may jet by mixing with anther organic solvent like tetralin, but stable jetting is not achieved. Actually, the nozzle plate has a hydrophobic surface energy designed for stable jetting of aqueous liquids. Here, we focus on processing of aqueous QD suspension.

The mechanical precision of the Dimatix DMP3000 falls within 5 μm. Inkjet printing of aqueous suspension of green QDs achieves a similar level of precision by solvent mixing or dilution. **Figure 18** shows an example of ink formulation and its correlation with jetting stability or precision of printing. QD1 is an aqueous QD suspension purified by centrifugation, also denoted as component A, while other constituents including a 28 wt% acetic acid, glycol, and DI water are denoted as component B, C, and D, respectively. The printing precision of each ink suspension is evaluated by the average deviation, which is calculated by equation (**1**), also shown in **Figure 17**. Deviation of each element single-drop film, r_{ij}, is dependent on the reference grid, which is also optimized by tuning an angle based on the least squares algorithm.

$$\bar{r} = \frac{\sum_{i=1}^{m}\sum_{j=1}^{n}\left|r_{ij}\right|}{m \times n} \tag{1}$$

http://dx.doi.org/10.5772/63425

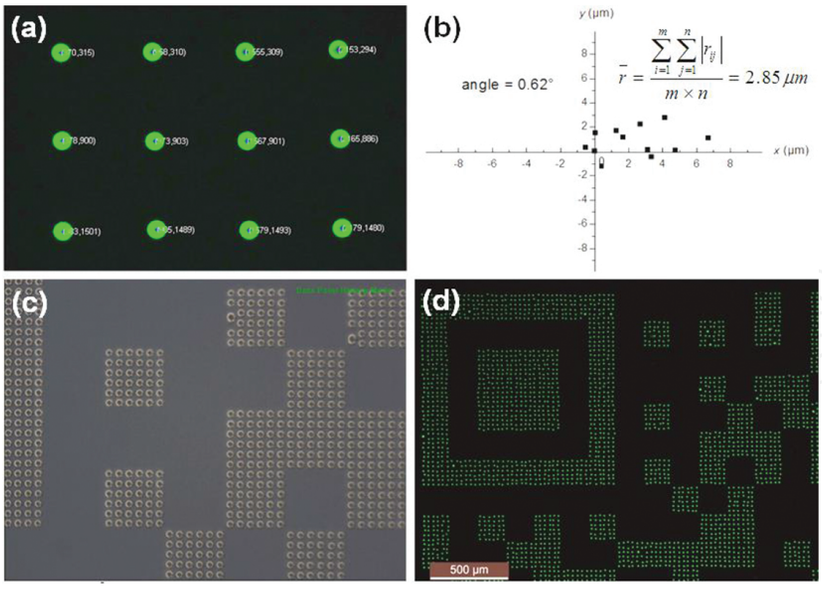

Figure 17. Calculation of positional deviation from target grid for ink jetting of CdSe QDs and demonstration of stable jetting (a) the florescent image of an printed QD single-drop film array with the coordinate extracted and marked as the raw data for calculation, (b) Statistics and calculation of average deviation, (c) an image captured with fiducial camera of the printer after printing a two-dimension code on SiO_2 and (d) fluorescent image of the two-dimension code.

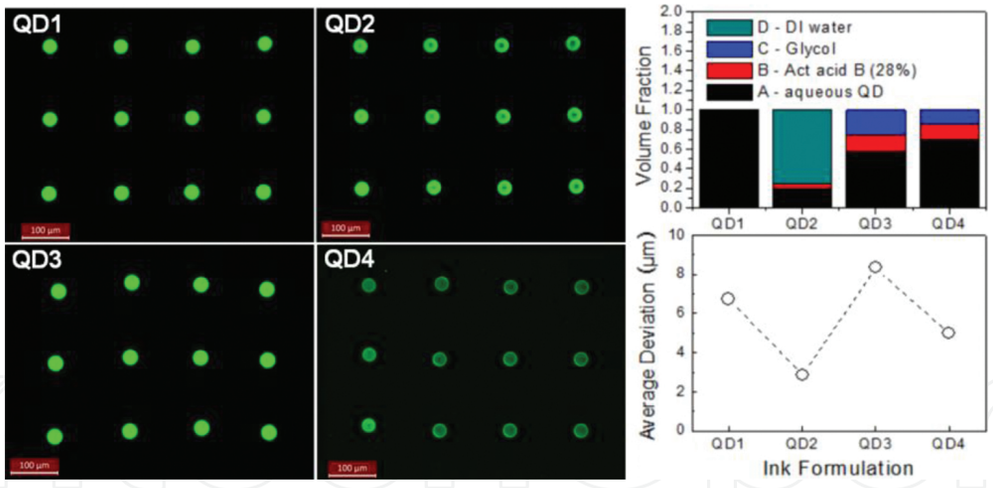

Figure 18. Correlation between ink formulation, color conversion efficiency, and jetting stability.

The aqueous QD suspension with pure component A can be printed with an average deviation of 6.74 μm. It can be remarkably improved to 2.85 μm by dilution with DI water and tuning the PH value with B to around 4. Mixing with ethylene glycol as component C negatively affects the jetting stability, but the high color conversion efficiency of the QDs was at least retained at a low PH value of 3.

Along with positional data for the evaluation of jetting stability, the distribution of the element film diameter in an array also conveys the information about the process stability. The element

QD film diameters can as well be extracted from corresponding fluorescent images for the study of the assembling behavior of QDs on an ITO substrate. Film arrays of green QDs are printed with multiple cycles at the same reference site of the substrate for accumulated assembling of QDs on the grid sites. As shown in **Figure 19**, the diameter of QDs on ITO increases abruptly with the number of printing cycles. Especially, comparing the average diameter obtained from the 3-layer and the 6-layer arrayed films, the doubled printing cycles achieves a 27.7% increase in diameter. The increase factor indicates three-dimensional assembling of QD on ITO. While on the ITO substrates that is patterned with inkjet-printed PVP film arrays, the assembling of QDs on these PVP underlying layer may undergo layer-by-layer assembling as the diameter is almost constant. It should be noted that the inkjet-printed PVP usually have coffee-ring profiles, which can be used as a bank to confine the posterior droplets of QD suspension. But in this experiment, the bank is not wetted owing to the relatively large diameter of PVP and the good positioning accuracy of both materials. Partial wetting of at the bank is observed for the 9-layer QD films printed on the 1-layer PVP, but instead of confinement, the bank guides the assembling of QDs along its interior sidewall. The diameters are calculated according to the area coverage of the fluorescent QDs. Partial wetting at the bank increases the coverage and accordingly increased the calculated film diameter showing an obvious deviation from the baseline data. This can be used for the detection of pattern misalignment.

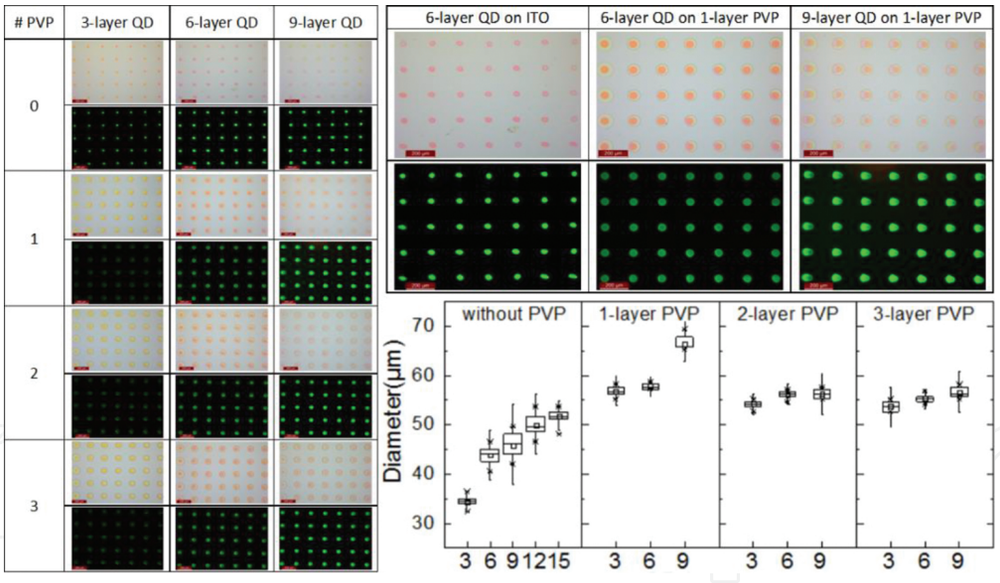

Figure 19. Modulation of the assembling behavior of QDs with inkjet-printed PVP underlying layers.

4. Conclusion

Small-molecule organic semiconductors can be readily processed via inkjet printing and other solution methods with the benefit of reduced cost and pollution. But it is noted that solution-

prepared devices are usually inferior in performance compared to their vacuum-prepared counterpart. Recent investigation on TIPS-PEN indicates a positive correlation between the single-drop film diameter and the dispersive component of the substrate's surface energy, while the coffee-ring staining can be explained by the polarity of surface energy. TIPS-PEN of uniform thickness is printed on the PETS-treated hydrophobic substrate. Process optimization across multiple dimensions is performed and high performance OTFTs are prepared. In addition to modulation of the thickness profile, the nucleation and film growth behavior can be effectively modulated as well. Transition from typical contact-line nucleation to interface nucleation is observed on the PETS-treated substrate, which is attributed to the nanoscale gradient of surface energy. Large-area continuous film with high surface coverage and high performance bottom-contact TIPS-PEN OTFTs can be fabricated on these hydrophobic substrates with nanoscale surface energy gradient. Surface energy also plays an important role in the printing of nanomaterials. Jetting stability, which is critically dependent on various surfaces, is qualitatively evaluated and employed as a key target of optimization for the printing of QDs. It can be employed for ink formulation. High resolution digital patterns are printed using QD material, which can be assembled in 3-dimensions or possibly stacked layer-by-layer depending on the underlying surface.

Author details

Xianghua Wang[1*], Miao Yuan[1,2*] and Mengzhi Qin[1,2*]

*Address all correspondence to: xhwang@hfut.edu.cn, horizon419@126.com and mzqin@foxmail.com

1 Academy of Photoelectric Technology, National Engineering Laboratory of Special Display Technology, National Key Laboratory of Advanced Display Technology, Hefei University of Technology, Hefei, China

2 School of Electronic Science & Applied Physics, Hefei University of Technology, Hefei, China

References

[1] D. Janssen, R. De Palma, S. Verlaak, P. Heremans, and W. Dehaen, "Static solvent contact angle measurements, surface free energy and wettability determination of various self-assembled monolayers on silicon dioxide," *Thin Solid Films*, vol. 515, pp. 1433–1438, 2006.

[2] C. Seungjun, K. Seul Ong, K. Soon-Ki, L. Changhee, and H. Yongtaek, "All-inkjet-printed organic thin-film transistor inverter on flexible plastic substrate," *IEEE Electron Device Letters*, vol. 32, pp. 1134-1136, 2011.

[3] J. Kim, J. Jeong, H. D. Cho, C. Lee, S. O. Kim, S. K. Kwon, *et al.*, "All-solution-processed bottom-gate organic thin-film transistor with improved subthreshold behaviour using functionalized pentacene active layer," *Journal of Physics D-Applied Physics*, vol. 42, pp. 115107-115112, 2009.

[4] A. Arias, S. Ready, R. Lujan, W. Wong, K. Paul, A. Salleo, *et al.*, "All jet-printed polymer thin-film transistor active-matrix backplanes," *Applied Physics Letters*, vol. 85, pp. 3304-3306, 2004.

[5] X. H. Wang, X. F. Xiong, L. Z. Qiu, and G. Q. Lv, "Morphology of inkjet printed 6, 13 bis (tri-isopropylsilylethynyl) pentacene on surface-treated silica," *Journal of Vacuum Science & Technology B*, vol. 30, pp. 021206-021211.

[6] S. Wu, *Polymer interface and adhesion*. New York: CRC, 1982.

[7] X. H. Wang, M. Yuan, X. F. Xiong, M. J. Chen, M. Z. Qin, L. Z. Qiu, *et al.*, "Process optimization for inkjet printing of triisopropylsilylethynyl pentacene with single-solvent solutions," *Thin Solid Films*, vol. 578, pp. 11–19, 2015.

[8] T. Sekitani, Y. Noguchi, U. Zschieschang, H. Klauk, and T. Someya, "Organic transistors manufactured using inkjet technology with subfemtoliter accuracy," *Proceedings of the National Academy of Sciences of the United States of America*, vol. 105, pp. 4976–4980, 2008.

[9] Y. H. Kim, B. Yoo, J. E. Anthony, and S. K. Park, "Controlled deposition of a high-performance small-molecule organic single-crystal transistor array by direct ink-jet printing," *Advanced Materials*, vol. 24, pp. 497-502, 2012.

[10] J. A. Lim, W. H. Lee, D. Kwak, and K. Cho, "Evaporation-induced self-organization of inkjet-printed organic semiconductors on surface-modified dielectrics for high-performance organic transistors," *Langmuir*, vol. 25, pp. 5404–5410, 2009.

[11] J. Fukai, H. Ishizuka, Y. Sakai, M. Kaneda, M. Morita, and A. Takahara, "Effects of droplet size and solute concentration on drying process of polymer solution droplets deposited on homogeneous surfaces," *International Journal of Heat and Mass Transfer*, vol. 49, pp. 3561–3567, 2006.

[12] M. Kuang, J. Wang, B. Bao, F. Li, L. Wang, L. Jiang, *et al.*, "Inkjet printing patterned photonic crystal domes for wide viewing-angle displays by controlling the sliding three phase contact line," *Advanced Optical Materials*, vol. 2, pp. 34–38, 2014.